Kinetic pathways of multiphase surfactant systems

M. Buchanan,* L. Starrs,* S. U. Egelhaaf, and M. E. Cates
Department of Physics and Astronomy, The University of Edinburgh, Mayfield Road, Edinburgh EH9 3JZ, United Kingdom
(Received 21 June 2000)

Relaxation following a temperature quench of two- (L_α and L_3) and three-phase (L_α, L_3, and L_1) samples has been studied in a sodium dodecyl sulfate–octanol-brine system. In the three-phase case we have observed samples that are initially mainly of the sponge phase, with lamellar and micellar phases on the top and bottom of the sample, respectively. Upon decreasing the temperature, most of the volume of the sponge phase is replaced by the lamellar phase. During equilibration we have observed three regimes of behavior within the sponge phase: (i) first there is disruption in the L_3 texture, then (ii) after the sponge phase homogenizes there is a L_α nucleation regime; finally (iii), a bizarre plume connects the L_α phase with the L_1 phase. The relaxation of the two-phase sample proceeds instead in two stages. First L_α drops nucleate in L_3, forming an onion ''gel'' structure. Over time the L_α structure compacts while equilibrating into a two-phase L_α-L_3 sample. We offer possible explanations for some of these observations in the context of a general theory for phase kinetics in systems with one fast composition variable and one slow.

PACS number(s): 05.70.Fh, 05.45.−a, 87.64.Rr

I. INTRODUCTION

The study of nonequilibrium phase behavior in complex fluid systems provides an interesting challenge. Specifically, in the case of surfactant systems, relaxation to equilibrium recently attracted interest [1–7]. For example, this was studied in phase penetration scan experiments [8–14] and in directional growth studies [15]. In these experiments the evolution of a mesophase is followed in the presence of a concentration or temperature gradient, respectively. This may result in unstable interfaces which can lead to spectacular instabilities.

The kinetics of phase behavior was well studied in other areas of soft matter physics. For example, the nucleation behavior in colloid-polymer mixtures was investigated experimentally and theoretically [16–21]. In these systems, three-phase samples consisting of colloidal gas, liquid, and crystal can be prepared at different compositions. In Refs. [17,20], three-phase samples were homogenized and observed while equilibrating. By identifying the fast and slow composition variables in the system, and then considering the evolving free-energy landscape for the slow component, restrictions can be placed on the kinetic pathway the system will follow as it evolves toward equilibrium. This free-energy landscape theory [17,21] promises to be a powerful way to predict kinetic pathways, at least in systems where one combination of the composition variables evolves more slowly than the others, so that time scales can be separated. It is used below (Sec. IV) to give a possible explanation for the observations in surfactant systems that will be presented here (Sec. III).

In this paper we investigate the temporal evolution of a two-phase system, comprising sponge (L_3) and lamellar (L_α) phases, and a three-phase system, comprising L_3, L_α, and micellar (L_1) phases, in samples that have been subjected to a temperature quench. Using dark-field *macroscopy* (explained below), we have observed a number of interesting nonequilibrium features that occur as the sample progresses to its new equilibrium state. In the two-phase sample we have observed dense nucleation of lamellar phase droplets within the L_3 phase, which appear to form a ''gel'' of droplets that compacts over time. In addition, we present microscopic images of the gel formation. In three-phase samples we observed three regimes of behavior. Initially the sponge phase forms an *emulsion* which proceeds to a homogeneous sponge phase. In the second regime nucleation of lamellar phase in the sponge phase occurs close to the L_3/L_1 interface. The growing droplets rise through the L_3 phase and arrive at the L_3/L_α interface, building up the L_α phase over time. Finally a *plume* pushes through the sponge phase connecting the L_1 and L_α phases. These results are described in Sec. III and discussed in Sec. IV. Section V gives a brief conclusion.

II. EXPERIMENT

A. Materials

Sodium dodecyl sulfate (SDS) and octanol (both 99% purity) were supplied by Sigma-Aldrich, and used without further purification. Samples were prepared by dissolving SDS and octanol in brine (20 g/l of NaCl in distilled water) and then tumbled for two days and subsequently allowed to equilibrate at a higher temperature of 40 °C. Experiments were performed after approximately two weeks, when the samples had reached equilibrium.

B. Dark-field macroscopy

Compared to a direct observation, dark-field macroscopy allows us to obtain better contrast from regions in the sample that scatter light only weakly [22,23]. The scattering of light is caused by refractive index inhomogeneities in the sample which, e.g., result from regions of different concentration.

*Present address: Centre de Recherche Paul-Pascal, CNRS UPR 8641, Avenue du Docteur-Schweitzer, F-33600 Pessac, France.

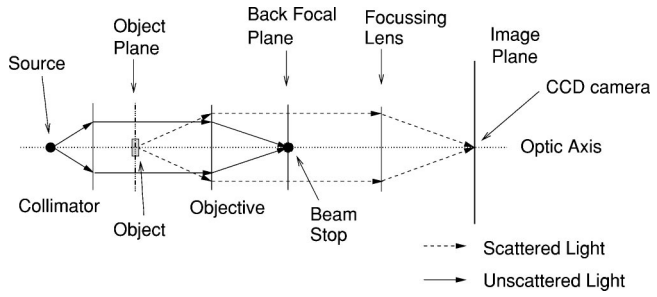

FIG. 1. Schematic diagram of dark-field macroscopy.

The term *macroscopy* is introduced since the sample is larger than its image, which matches the size of the charged-coupled-device (CCD) chip, and therefore the optical setup, is designed to *reduce* the image size. We have used dark-field macroscopy to observe samples whose cell dimensions are $4\times1\times1$ cm^3.

The general layout of the dark-field macroscope is similar to a dark-field microscope, and is shown in Fig. 1. A white light source and a collimator are used to produce parallel light to illuminate the sample, which is placed in the object plane. The unscattered light is focused into the back focal plane of the objective. A beam stop is placed in this plane to block the unscattered light. In the case of no scattering the image is completely dark; hence the name ''dark field.'' If there is scattered light, it is collimated by the objective and focused onto the CCD chip. Therefore, whenever there are refractive index differences in the sample these will appear as bright spots on a dark background. All samples observed are temperature controlled in a heat bath.

C. Microscopy

All microscopy observations were made using an Olympus BX50 microscope in bright-field mode between crossed polarizers with long working distance objectives. The evolution of the samples were recorded using a CCD camera and time lapse video recorder together with a framegrabber personal computer. The contrast of the presented images was enhanced by thresholding. All microscopy experiments were done in a Linkam hot stage, which ensured a controlled and stable temperature.

III. RESULTS

We have studied two-phase (L_α,L_3) and three-phase (L_α,L_3,L_1) samples upon a large temperature change. Initially the samples are in equilibrium at $T=40\,^\circ$C, where they have been observed for one week and showed no further change. The sample is then placed in the dark-field macroscope, which is kept at a temperature of $20\,^\circ$C. Its behavior upon this temperature quench is then followed. We have studied samples with different bilayer (SDS + octanol) concentrations and octanol-SDS ratios. We will first present the typical behavior of two- and three-phase samples, before we describe the dependence on the octanol-SDS ratio.

A. Two-phase samples

1. Macroscopic observations

Temperature quench experiments on a two-phase sample (L_α,L_3) were performed for an octanol-SDS ratio of 1.36 and a bilayer concentration of 30%. At this composition and at a temperature of $40\,^\circ$C, the sample has two phases, L_α at the top and L_3 on the bottom, where the L_3 phase is in abundance ($\sim$95%). At lower temperature ($T=20\,^\circ$C) most of the volume ($\sim$70%) of the sample is present as the L_α phase, which replaces the L_3 phase.

When the sample is quenched from $T=40$ to $20\,^\circ$C, we have observed two regimes of behavior. Almost immediately, (L_3+L_α) nucleates in the L_3 phase, and appears to completely fill the sample [Fig. 2(a)]. Over time this mixed sponge-lamellar phase decreases in volume, and the ''pure'' sponge phase now reforms at the bottom of the sample [Fig. 2(b)]. As the volume of (L_3+L_α) decreases there is a noticeable change in its texture. The lower part is rough in texture and separated by an interface from the top part which has a smooth texture [Fig. 2(c)]. The rough texture appears to be a gel of L_α droplets in L_3; this is confirmed by micros-

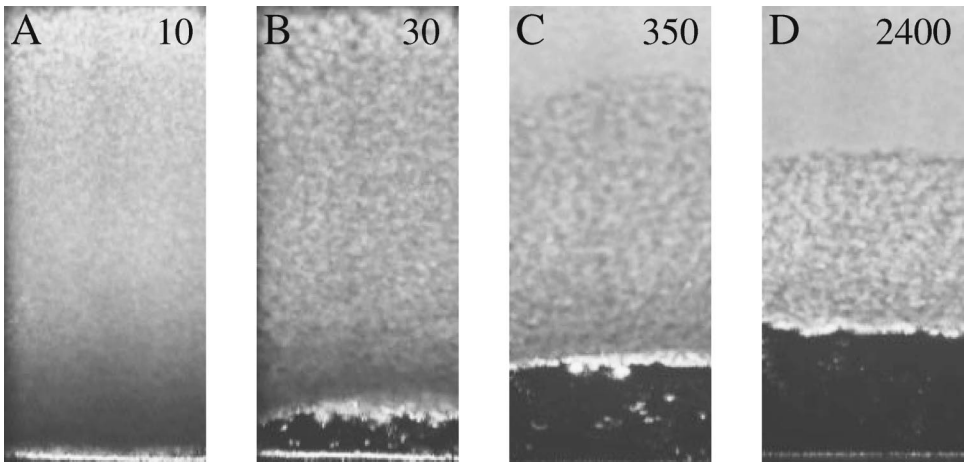

FIG. 2. Temperature quench from $T=40$ to $20\,^\circ$C of a two-phase sample. (a) Immediately after the temperature quench, a mixture of L_3 and L_α phases appears to fill the sample completely. (b) Its volume begins to decrease, and a ''pure'' sponge phase is observed at the bottom of the cell. (c) and (d) Two textures of lamellar phase are observed: rough (middle) and smooth (top). The smooth part increases in volume as the rough part decreases over time. (Times are displayed in minutes.)

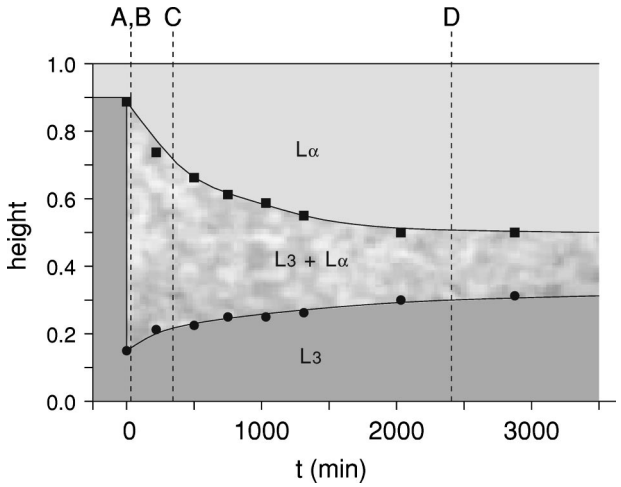

FIG. 3. Schematic temporal profile of lamellar (L_α) and sponge (L_3) phases in a two-phase sample. The $L_\alpha/(L_\alpha+L_3)$ interface (filled squares) is determined by the difference in smooth and rough textures. Likewise the $(L_\alpha+L_3)/L_3$ interface is marked by ●.

copy observations (see below). Over time the smooth part grows as the rough part shrinks [Figs. 2(c) and 2(d)]. The final state of the sample (not shown) contains only a smooth lamellar phase in peaceful coexistence with the sponge phase, where the two phases occupy comparable volumes of the sample.

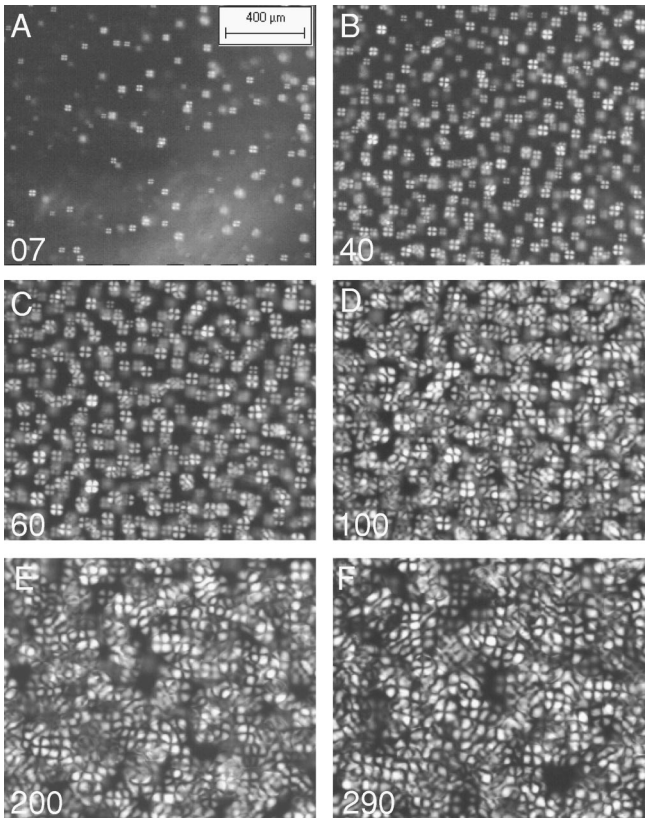

FIG. 4. Micrographs of the nucleation and gelation of droplets of L_α (onions) in the L_3 phase. (a)–(c) Onions nucleate homogeneously in the L_3 phase and then proceed to grow. (d)–(f) Subsequently onions move toward each other, forming a ''gel'' network of onions; voids of L_3 phase can be clearly observed. All images viewed through crossed polars. (Times are shown in minutes.)

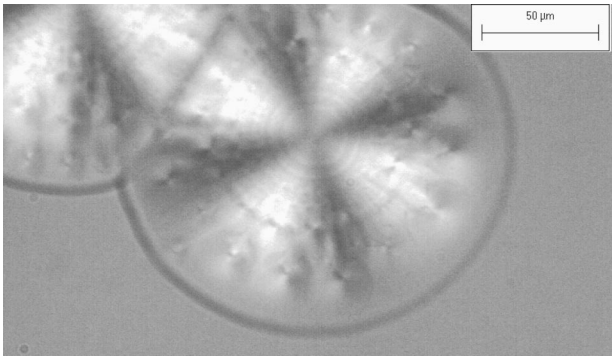

FIG. 5. Onions that have nucleated in the L_3 phase after a temperature quench, and then partially coalesced. Note the distinctive pattern of focal conic defects.

The same generic behavior is observed in samples with octanol-SDS ratios up to 1.44 at 30% bilayer concentration. In Fig. 3 the relaxation to equilibrium observed with these samples is schematically presented.

2. Microscopic observations

To obtain more detailed information, part of the sponge phase was extracted from a two-phase sample. It was subsequently observed with a microscope during a temperature ramp from $T=40$ to 20 °C. Droplets of the L_α phase, which have the birefringent ''Maltese cross'' signature of multilamellar vesicles or onions, are observed to nucleate homogeneously in the L_3 phase. These droplets continue to grow to 10–50 μm over the next 60 minutes [Figs. 4(a)–4(c)]. However, after 30 min the onions start to move toward each other, forming an onion gel [Fig. 4(d)]. This structure coarsens over time, leaving voids of pure sponge phase [Figs. 4(e) and 4(f)]. As more onions form in the L_3 phase, they coalesce. The heterogeneity of the gel is presumably responsible for the rough texture reported above.

Figure 5 shows a close-up of two droplets, with Maltese crosses visible, when observed through partially crossed polars. In this case the two droplets have partially merged. On closer inspection these lamellar droplets have a distinctive pattern of focal conic defects that form within the onion [Fig. 6(a)]. These defects in the onion are presumably due to an epitaxial tilt of the bilayers at the surface of the droplet, which is surrounded by a sponge phase. This has also been observed at the interface between homeotropic lamellar and sponge phases [24]. The epitaxial tilt is required to match the repeat distance in the lamellar phase onto the characteristic

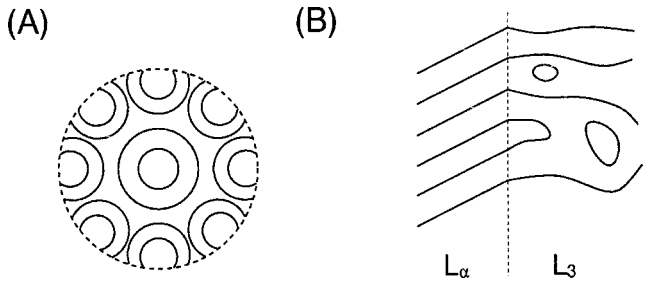

FIG. 6. (a) Schematic diagram of an onion in the L_3 phase, where focal conic defects form in the onion to satisfy an epitaxial tilt at the L_α/L_3 interface, as shown in (b).

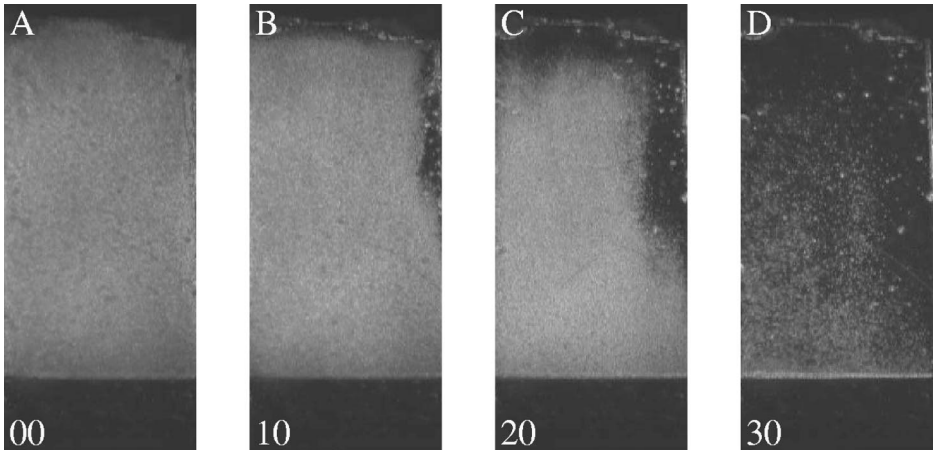

FIG. 7. Initial stages of a temperature quench on a three-phase sample. The L_α phase is at the top (it appears dark here), the L_3 phase in the middle, and the L_1 phase at the bottom (it appears dark). (a) Disruption appears immediately after the quench [(b) and (c)] which clears over a 1-h period. Times are shown in minutes.

bilayer spacing in the sponge [Fig. 6(b)]. This observation suggests that, at the observed temperature and time scales, the internal structure of each onion is capable of reorganizing to minimize the interfacial energy of the onion.

B. Three-phase samples

Samples within the three-phase region have been observed with 5% and 10% bilayer concentration over a range of octanol-SDS ratio 1.22 to 1.32. At these compositions and at $T=40\,^{\circ}\mathrm{C}$, all samples consist of three phases: L_α at the top, L_3 in the middle, and L_1 on the bottom, where the L_3 phase has the largest volume. At a lower temperature of $20\,^{\circ}\mathrm{C}$ most of the volume is occupied by the L_α phase, with only a small volume of L_3 phase remaining. The L_1 phase is observed to have a slightly larger volume at $T=20\,^{\circ}\mathrm{C}$ than at $40\,^{\circ}\mathrm{C}$. After a temperature quench from $T=40$ to $20\,^{\circ}\mathrm{C}$ the relaxation to equilibrium is found to proceed through three regimes. They are described below for a sample that has a bilayer concentration of 5% and an octanol-SDS ratio of 1.22. Other three-phase samples behave in a similar fashion, although the time constants were found to depend on the actual composition.

1. Early stages

After the temperature quench, the L_3 phase becomes turbid as inhomogeneities form within it [Fig. 7(a)]. This texture appears to be an emulsion of L_1 droplets separated by an L_3 phase, or vice versa (see Sec. IV for a discussion). The texture is first seen close to the L_1/L_3 interface, and then spreads up to the L_3/L_α interface, while large convection currents are also observed within the L_3 phase.

In addition some large droplets of the L_1 phase fall rapidly from the L_α phase through the inhomogeneous L_3 phase into the L_1 phase (Fig. 8). These droplets are initially of a diameter of about 90 μm, and fall with a speed $\sim 1000\ \mu\mathrm{m\,s^{-1}}$. Within 3 h their size decreases to $\sim 14\ \mu$m and their speed is reduced to $\sim 15\ \mu\mathrm{m\,s^{-1}}$. About 1 h later the L_3 phase becomes homogeneous once again, by a clearing process which starts close to the L_3/L_α interface. A schematic summary of these features is given in Fig. 9. These features are typical of samples at a 5–10 % bilayer composition with octanol-SDS ratios 1.22–1.32.

2. Lamellar nucleation and growth

After about 1 h droplets of the L_α phase of approximately 10–20 μm in size begin to form in the L_3 phase. The number of L_α phase drops observed increases over the next 30 min. While droplets are observed to nucleate throughout the L_3 phase, this mainly happens near the L_1/L_3 interface (Fig. 10). The droplets move up toward the L_α phase with a speed of about $4\ \mu\mathrm{m\,s^{-1}}$, gaining size as they do so. Over a period of 1–2 days they build the L_α phase. The quantity of the L_α phase steadily increases, however after 12 h the number of droplets within the L_3 phase is observed to have decreased. Eventually after about 36 h further droplets are not observed

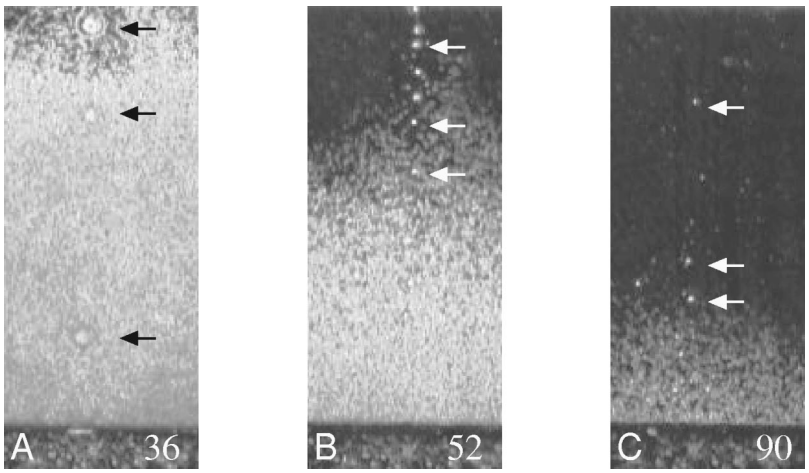

FIG. 8. Droplets of the L_1 phase (indicated by arrows) nucleate in the L_α phase and fall through the L_3 phase. The L_α phase is on top of the L_3 phase, and is not shown in this closeup. (Times are shown in minutes.)

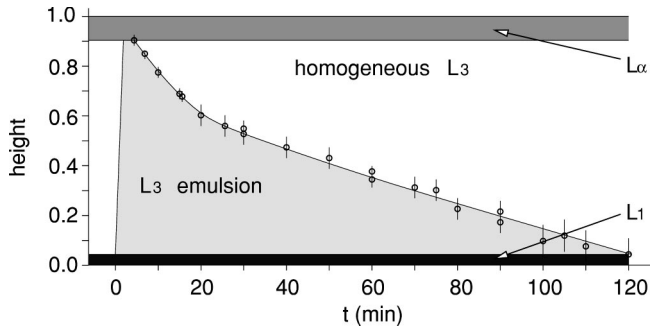

FIG. 9. Temporal evolution of the sample, in particular the sponge emulsion, during the early stages. This sample contains a higher bilayer concentration of 8% than the samples in Figs. 7 and 8; while the generic behavior is the same, the observed kinetics are slower. The sponge emulsion texture is shown as the shaded region in the diagram. The error bar indicates the width of the interface.

to form despite the continuing growth of the lamellar phase. These findings are summarized schematically in Fig. 11.

At larger bilayer concentrations (30–40 %) we have observed a much larger density of lamellar droplets in the L_3 phase. At much larger octanol-SDS ratios of 1.35 and 1.41, the droplets that form are very dense. Furthermore, by increasing the octanol-SDS ratio, we have observed a noticeable change in the dynamics. At a higher octanol-SDS ratio we observe an increase in the rate of formation of the L_α droplets and the speed of the droplets as they move toward the L_α phase.

3. Plume

After 36 h the L_α droplets are no longer observed to nucleate in the L_3 phase. However, the L_α phase still continues to grow. Eventually at some later time a plume grows from the L_1 phase, and extends up to the L_α phase (Fig. 12).

Prior to this, in the L_1 phase small droplets of L_α phase are observed to move up toward the L_3/L_1 interface, and eventually push their way through the L_3 phase by forming the plume. The plume connects the L_1 phase to the L_α phase, cutting straight through the L_3 phase. It is about 50–100 μm in diameter. On the plume near the L_1/L_3 interface a large bulbous piece with a diameter of about 100 μm can be observed. We followed the movement of this over the next 12 h. Initially the bulbous piece rises up toward the L_α/L_3 interface [Figs. 12(b) and 12(c)]. Then it begins to move back toward the other interface [Figs. 12(c)–12(e)]. Eventually the plume detaches from the L_3/L_1 interface, and the whole plume is ''pulled'' up into the L_α phase [Figs. 12(e)–12(g)], while the bulbous bit remains at the loose end of the plume. The only way to describe the motion of the plume is that it behaves in a ''lava-lamp-like'' fashion.

The occurrence of the plume is a reproducible effect, and has been seen in many separate experiments. However, in the range of samples we have observed we only find plumes when the L_1 phase is present. Depending on the composition we can even observe multiple plumes forming. The plumes are observed late in the lamellar nucleation regime. However, at larger octanol-SDS ratios plumes form earlier in the

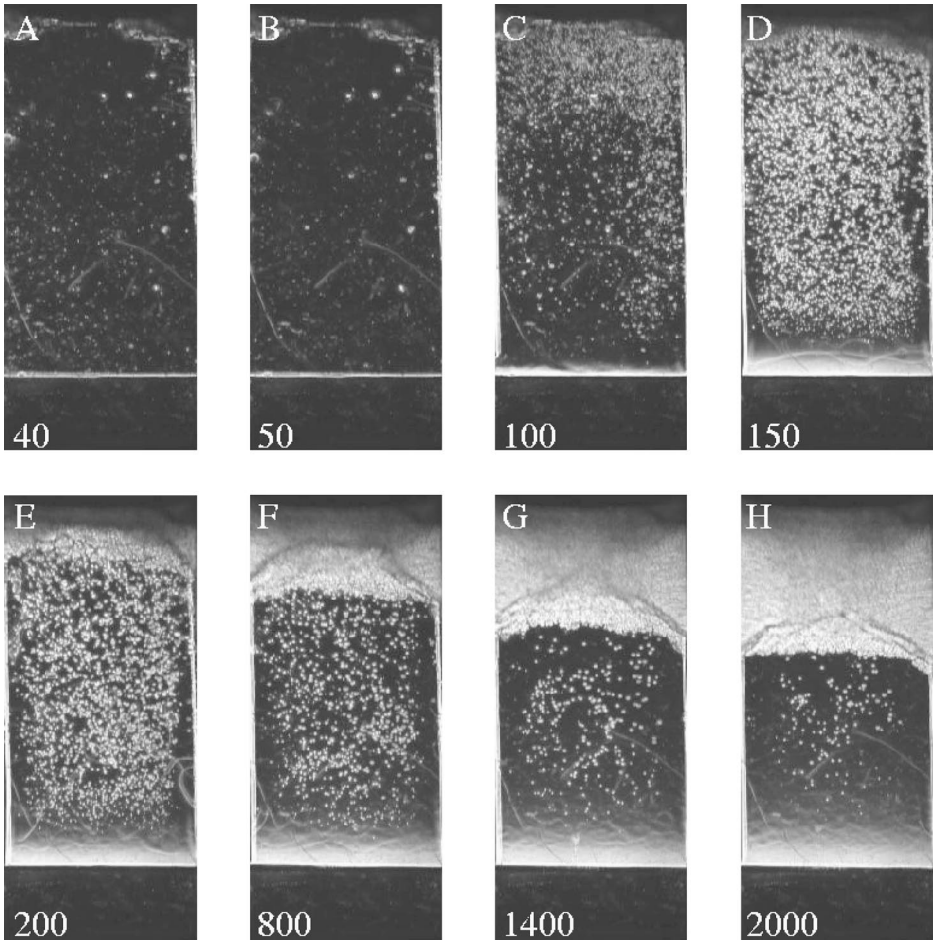

FIG. 10. Birefringent droplets form in the sponge phase L_3 (middle) as the lamellar phase L_α (top) grows. (a) and (b) The initial sample settled in a homogeneous phase. (c)–(f) The L_α droplets nucleate in abundance, but mainly near the lower (L_1/L_3) interface. The droplets rise to the L_3/L_α interface, building the L_α phase. (g) and (h) L_α drop nucleation slows down and eventually stops, although the lamellar phase continues to grow. Times are shown in minutes.

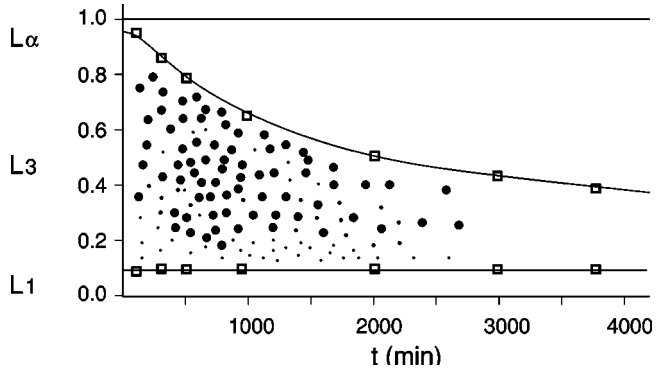

FIG. 11. Temporal evolution of the density of lamellar phase droplets in the sponge phase. The positions of the L_1/L_3 and L_3/L_α interfaces are given (□). Freshly nucleated droplets (●) are observed to nucleate mainly near the L_1/L_3 interface. As droplets grow and move toward the L_α phase, their density (●) appears to be fairly uniform.

L_α nucleation regime. In addition, we have observed streaks in the L_3 phase at the L_α interface, which persist for the remaining duration of the growth of the L_α phase. They are found during and after the formation of the plume.

4. Octanol-SDS dependence

As already mentioned in Sec. III B 2, a higher octanol-SDS ratio also results in an increase in the rate of formation of the L_α droplets and the speed of the droplets as they move toward the L_α phase. In addition, the density of droplets is increased upon an increase in the octanol-SDS ratio. By varying the octanol content in the bilayer we influence the time scale of each regime that is observed. The initial regime, where we have observed the transient formation of a sponge emulsion, appears to persist for a shorter period of time as we increase the octanol-SDS ratio.

This is also the case for the second regime of lamellar nucleation and growth. Furthermore, the nucleation regime starts earlier for samples with higher octanol content, so that these regimes overlap. This is also the case for the observation of the plume which can be observed earlier at a higher octanol-SDS ratio. Figure 13 gives a semiquantitative diagram of these observations.

IV. DISCUSSION

An initially equilibrated sample, that is subjected to a sudden temperature change will relax to a new equilibrium state. In three- and two-phase surfactant samples, we have observed interesting behaviors as the samples proceed to this final equilibrium state. Below we discuss these observations first for the three-phase sample and then for the two-phase sample. This will be followed by some possible explanations for the observed behavior.

A. Early stages

When the three-phase sample is quenched from $T=40$ to 20 °C, the L_1 phase volume is found to increase during the early stages. This indicates that during the quench the majority phase L_3 increases its bilayer concentration with a concomitant reduction in its bilayer spacing, expelling the L_1 phase. This would explain the formation of a ''sponge emulsion,'' which appears as an inhomogeneous texture (Fig. 7). A minority of L_1 phase in the sponge phase was previously

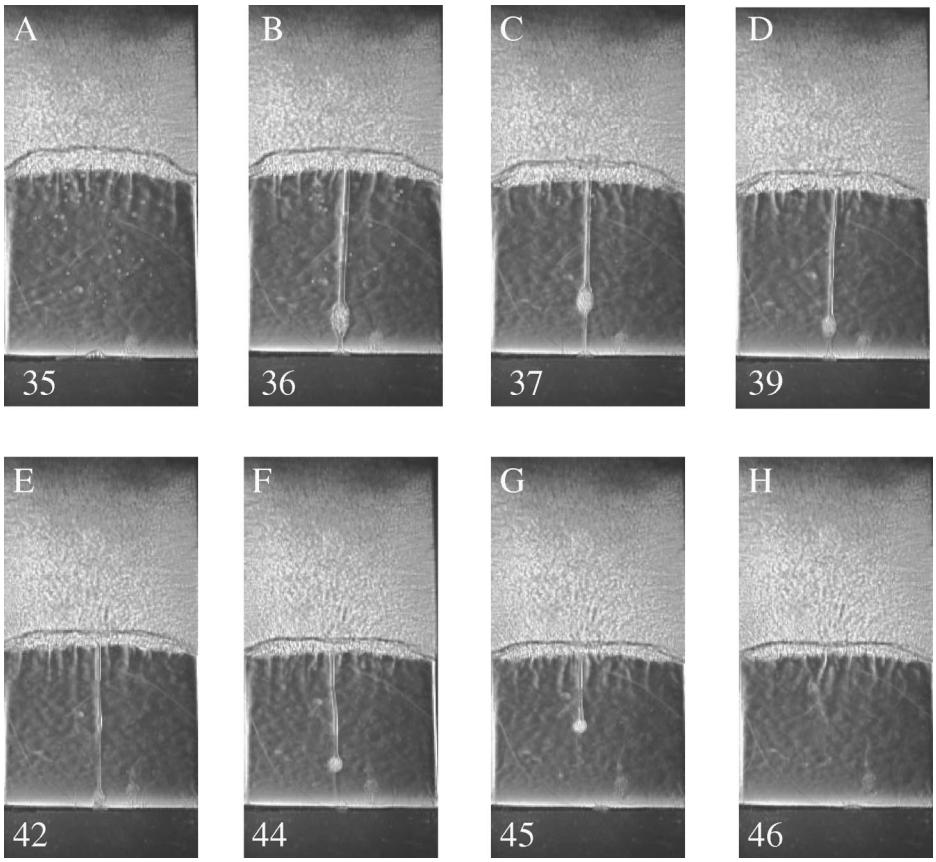

FIG. 12. A bizarre plume forms at the L_1/L_3 phase interface, and grows to the lamellar phase. Times are shown in hours.

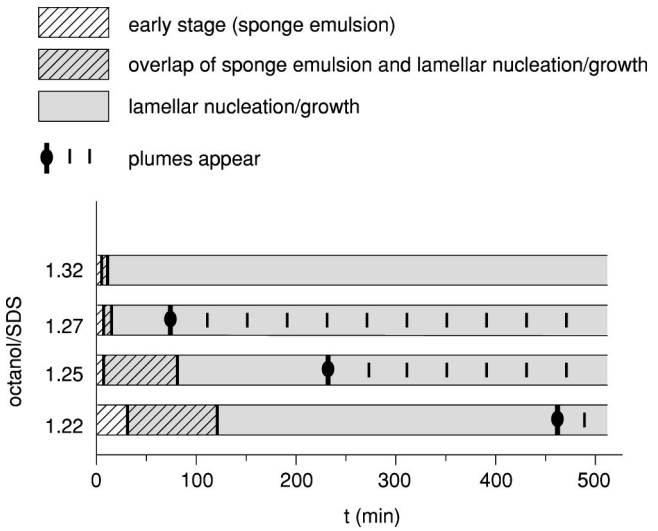

FIG. 13. Dependence of the temporal evolution of the different regimes on the octanol-SDS ratio. The duration and onset time of these features are also dependent on this ratio. The total bilayer concentration is 10%.

observed in other experiments [25,26]. Furthermore, the subsequent separation of L_1 and L_3 phases may lead to the observed convection currents. The sample begins to homogenize again as the compositions reorganize into a more favorable state. The homogenization of the L_3 phase is found to start at the L_α phase, and to move toward the L_1 phase. This is not surprising, since the L_1 phase has to drain through the sponge emulsion during the homogenization process (Fig. 7).

A similar decrease in bilayer spacing is also expected for the L_α phase. Consequently the bilayer concentration will increase, and excess brine will be expelled, possibly together with a low concentration of surfactant and cosurfactant. It seems conceivable that this leads to the formation of droplets of L_1 within L_α, which are then observed to fall through the L_3 phase (Fig. 8). As the equilibrium bilayer concentration is approached, the L_1 flux is reduced. This is reflected in the reduction of the L_1 droplet size, and consequently leads to a reduction in the speed of the droplets.

By expelling excess brine, both the L_3 and L_α phases increase their bilayer concentration. The decrease in undulation repulsions between layers as a result of the lowered temperature seems likely to be responsible for this behavior [27]. This change in bilayer concentration occurs during the early stages, and appears to be much faster than reorganization within the bilayer. The slower intrabilayer reorganization is thus expected to influence the behavior during subsequent stages.

B. Lamellar nucleation and growth

After the early stage described above (and sometimes overlapping with it—see Fig. 13), a lamellar phase is found to nucleate and grow within the L_3 phase at the expense of the sponge phase. One of the most striking features of this process is that the nucleation of the L_α phase in the L_3 phase is not homogeneous throughout the L_3 phase, but is most abundant close to the L_1/L_3 interface. It seems peculiar that such nucleation should occur in the part of the L_3 region

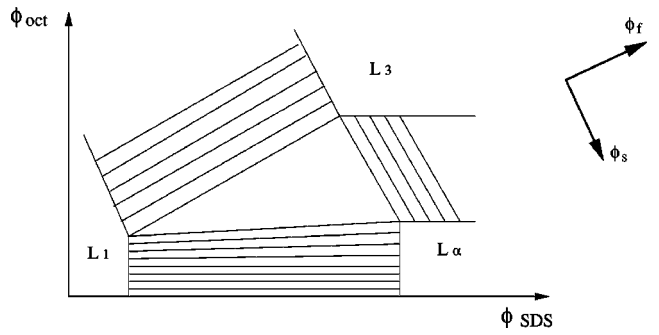

FIG. 14. Schematic phase diagram of the SDS-octanol-brine system close to a three-phase region consisting of lamellar (L_α), sponge (L_3), and micellar (L_1) phases. The direction of increasing bilayer volume fraction ϕ_f and relative amount of octanol in the bilayer ϕ_s are also shown.

furthest from the existing slab of L_α phase. A possible explanation for this can be found by analyzing the way the free energy landscape changes after the temperature jump [17,21].

First let us consider a three-phase sample (L_1,L_3,L_α) at equilibrium. To our knowledge there is no published phase diagram for this system that would show the phase boundaries close to the three-phase region. However, from our experience with these samples we present a schematic phase diagram of this region as a function of the volume fraction of SDS ϕ_{SDS} and octanol ϕ_{oct} (Fig. 14).

Figure 15 gives a schematic free energy landscape that is consistent with the observed phase diagram of the system. The free energy of the sample in equilibrium is a function of the volume fractions of two independent components, SDS and octanol.

At equilibrium the chemical potentials ($\mu_{\mathrm{SDS,oct}} = \partial f / \partial \phi_{\mathrm{SDS,oct}}$) of each component must be equal in all of the coexisting phases, $\mu^{L_1}_{\mathrm{SDS,oct}} = \mu^{L_3}_{\mathrm{SDS,oct}} = \mu^{L_\alpha}_{\mathrm{SDS,oct}}$. The same also applies to the osmotic pressure of each phase. This means that the tangents (shaded plane, Fig. 15) to the free energy ''wells'' at the equilibrium compositions will all be the same. The points of tangency will correspond to the corners of the three-phase triangle on the phase diagram (Fig. 14).

Note that this analysis is invariant under an arbitrary linear combination of the composition variables. Here we will

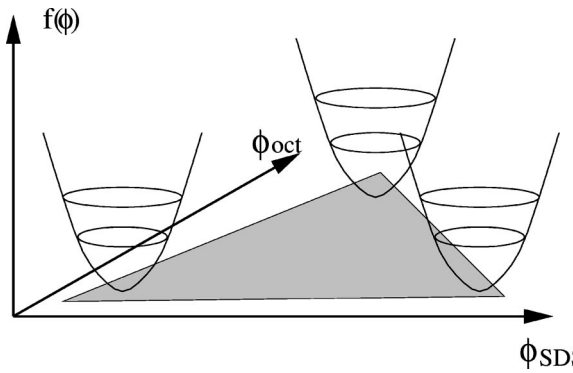

FIG. 15. Free energy landscape for an equilibrated two-component system [$f(\phi_{\mathrm{oct}},\phi_{\mathrm{SDS}})$] under conditions where three phases exist. The shaded plane represents the tangent plane.

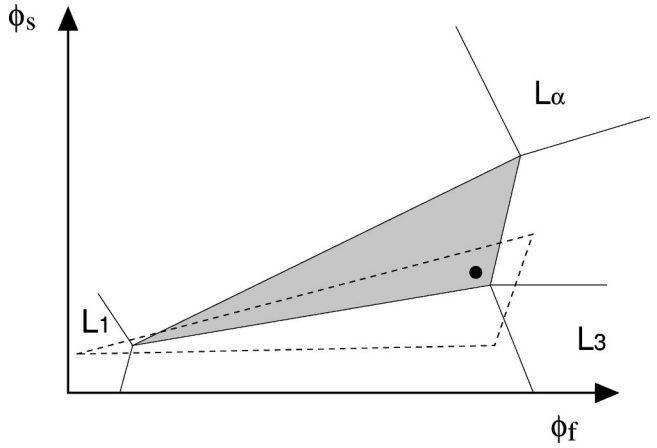

FIG. 16. Schematic phase diagram close to the three-phase region for two different temperatures. The solid lines and the gray area represent the three-phase region at high temperature. Upon a decrease in temperature the three-phase region moves to the position indicated by the dashed lines. Phases denoted are micellar (L_1), sponge (L_3), and lamellar (L_α) phases. The composition of the sample discussed in the text is indicated by ●.

choose linear combinations ϕ_f and ϕ_s as indicated in Fig. 14. (These are related to the volume fraction of bilayer and the composition of the bilayer, respectively, as we discuss below.) With these as the densities, the phase diagram looks like Fig. 16.

Now we ask how a three-phase sample (marked in Fig. 16 by ●) changes upon a temperature quench. Suppose at a given temperature its composition is close to the L_3 corner of the three-phase triangle (gray area in Fig. 16). It thus mainly consists of L_3 phase, but also contains small amounts of L_α and L_1 phases. Upon a change in temperature the free energy landscape rearranges such that the free energy minima move to new positions. This changes the position of the three-phase triangle (dashed lines in Fig. 16). Although the chemical composition of the sample remains constant, its relative position in the three-phase region is changed. In the case shown, it is now located much closer to the L_α corner, and also moved toward the L_1 corner. The sample is thus forced to change its compositions locally and nucleate L_α and L_1 phases at the expense of the L_3 phase. This is what happens in our three-phase samples when we quench from 40 to 20 °C.

Following Ref. [17], a quasiequilibrium free energy landscape can be constructed after the temperature quench if fast and slow composition variables can be identified. Application of this *free energy landscape* analysis to our system depends on the relation between the fast and slow components (ϕ_f, ϕ_s) and the volume fractions of octanol (ϕ_{oct}) and SDS (ϕ_{SDS}). Our observations indicate that changes in the bilayer concentration occur during the early stages, and can thus be identified with the fast component. In contrast, changes in the organization of the bilayer such as the transition from L_3 to L_α are found to happen later. From the phase diagram (Fig. 14), it is clear that this L_3-L_α transition must involve changes in the bilayer composition (at nearly constant bilayer fraction). This is also supported by our separate observations of contact experiments between the lamellar phase and water, where myelin patterns form [26,28].

Immediately after contact the myelin formation is always observed before the formation of any other intermediate phase, such as the L_3 phase. Thus the time for bilayers to swell to the miscibility gap is faster than the formation of a sponge phase, which requires local reorganization in the bilayer structure, and also a change in its composition.

We therefore assume that, starting from a given initial state, changes in the volume fraction of the fast component ϕ_f correspond to changes in the total bilayer concentration at a fixed SDS-octanol ratio. (This is expected to be a fast, ''collective diffusion'' mode.) We also assume that the slow component corresponds to changes in the SDS-octanol ratio at a roughly fixed bilayer volume fraction. This second assumption is physically reasonable, but less obvious: formally; the fast and slow directions are eigenvectors of a diffusion matrix, which need not be symmetric, and they need not be at right angles. However, if we make both assumptions, the fast and slow directions correspond to radial and tangential directions in Fig. 14, which is probably a good enough approximation for the present discussion. For a state near the L_3 corner initially, these are as indicated in the figure.

For the fast component, the chemical potential $\mu_f = \partial f / \partial \phi_f$ will become uniform rapidly. Essentially, we move to an equilibrium state through a sequence of metastable states, for which the chemical potential of the fast component μ_f is uniform. However, the value of μ_f is evolving in time, and depends on the (nonuniform) evolution of the slow variable ϕ_s. Instead of drawing the free energy landscape as a function of two components (Fig. 15), we now concentrate on the slow variable ϕ_s only. [This defines a free energy $f(\phi_s, \mu_f)$ as a function of ϕ_s in a semigrand ensemble, under conditions of uniform, but time dependent,

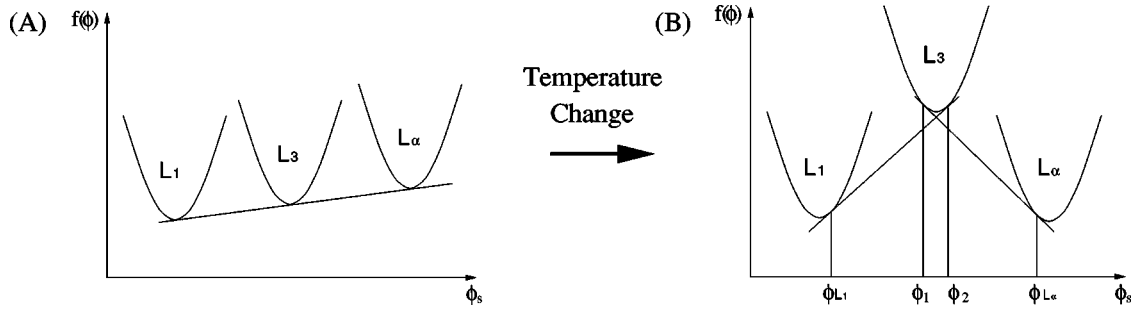

FIG. 17. Free energy landscape of a three-phase sample (A) in equilibrium at high temperature, and (B) during relaxation to a new equilibrium after a temperature quench

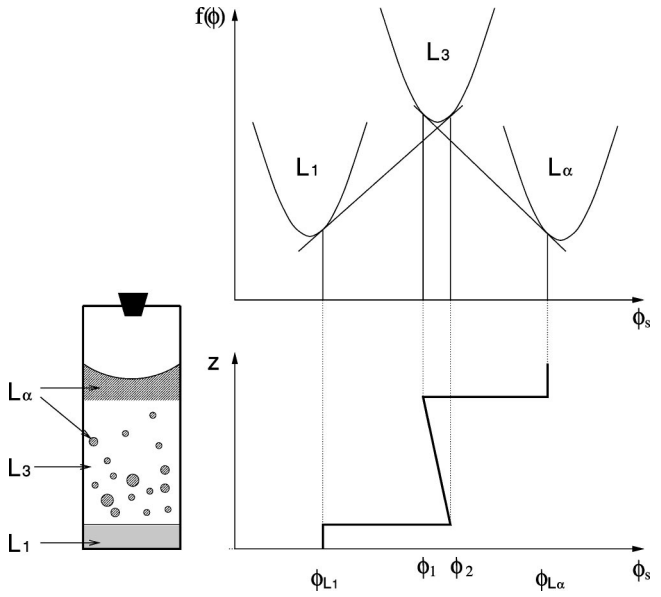

FIG. 18. Schematic diagram of a three-phase sample showing the nucleation of the L_α phase in the L_3 phase near to the L_1/L_3 interface, and its composition profile as a function of sample height z as deduced from the free energy landscape as a function of the slow component ϕ_s.

μ_f.] Figure 17(A) shows the initial (equilibrium) free energy landscape at high temperature as a function of the slow composition variable. After a temperature quench the three minima do not have a common tangent [Fig. 17(B)], since μ_f has not yet relaxed to its equilibrium value and the initial condition now represents a metastable state. In this diagram we may assume that the free energy curve of the L_3 phase lies higher than the common tangent of the other two, so as to favor producing more L_1 and L_α phases. (If the free energy minimum of the L_3 phase is below the tangent of the other two, then no nucleation will occur. In fact, this would be the case where the change in phase diagram is in the opposite direction to the one shown in Fig. 16.) Once the sample reaches equilibrium at the lower temperature, the three minima again have a common tangent [a situation similar to that in Fig. 17(A) is recovered].

The local composition of the phases near their interfaces with one another can be determined from the *metastable common tangents* to the free energy landscape [Fig. 17(B)]; the compositions at each end of a tangent have the same chemical potential μ_s of the slow component, which is the condition for *local* equilibrium of the interface. From these tangents, the local composition of the L_3 phase near to its interfaces can be determined. The L_3 phase will reorganize to have two different compositions, $\phi_s=\phi_1$ near the L_α/L_3 (upper) interface and $\phi_s=\phi_2$ near the L_3/L_1 (lower) interface. The L_3 phase thus has a higher bilayer volume fraction nearer the L_3/L_1 interface. The resulting composition profile as a function of sample height z is shown in Fig. 18. Since the nucleation of the L_α and L_1 phases will be induced by composition fluctuations in the L_3 phase, the L_α phase is more likely to nucleate close to the L_3/L_1 interface with its higher volume fraction. The difference in concentrations at the two interfaces requires a concentration gradient across the L_3 phase. Since $\phi_1<\phi_2$, then the upper part of the phase has higher mass density than the lower part. (This could cause the system to become unstable under gravity.) The concentration gradient as well as gravity favors driving the L_α droplets up toward the L_α phase.

Note that these features directly depend on the presence of the L_1 phase, which fixes $\phi_s=\phi_2$ at the bottom of the sponge phase. Also, the inversion of the concentration profile predicted by this model follows directly from the fact that the homogeneous L_3 region in the initial state is metastable: its common tangents to L_1 and L_α phase cross each other [Fig. 17(B)].

C. Plume

The formation of a plume which extends from the L_1/L_3 interface into the L_α phase appears to result from the nucleation of lamellar phase in the L_1 phase. The formed lamellar phase might build up at the L_1/L_3 interface, because the density difference between L_α and L_3 phases is very small and the surface tension between L_α and L_3 phases is large. Eventually the L_α phase formed in the L_1 phase pushes through the sponge phase in a lava-lamp-like fashion.

D. Comparison of two- and three-phase samples

The absence of the L_1 phase leads to a clearly different relaxation behavior of the two-phase samples, although for both kinds of samples the main change upon a temperature quench from $T=40$ to 20 °C is the formation of the L_α phase at the expense of the L_3 phase. There is no indication of the formation of a (metastable) L_1 phase within the L_α or L_3 phases during the early stages, as observed for the three-phase samples. This could, however, be due to the large octanol-SDS ratio of the two-phase samples, which leads to an overlap of the early stages and the lamellar nucleation in the case of the three-phase sample (Fig. 13), and could mask the (intermediate) formation of the L_1 phase.

In the case of the two-phase samples, the nucleation of the L_α phase occurs homogeneously throughout all of the L_3 phase. Since only one interface (L_α/L_3) is present, the L_3 phase cannot develop a density inversion which could influence the local nucleation rate. The quantity of nucleating L_α phase is large due to the relatively high bilayer concentration (30%). The nucleated L_α droplets (onions) appear to form a dense network in the L_3 phase (Fig. 4), similar to a colloidal gel structure. This is followed by a compaction process, which could be viewed as the drainage and collapse of a gel of L_α droplets in the L_3 phase. (For analogous phenomena in colloids, see Refs. [23,22].) Due to the lower mass density of the L_α phase, the onion gel collapses toward the upper phase boundary of the L_3 phase. This results in the observed smooth texture above the still uncompacted onion gel in the L_3 phase with its rough texture (Figs. 2 and 3). This is reminiscent of the creaming of emulsions. The final equilibrium state of the two-phase samples consists of a completely compacted lamellar phase and a ''pure'' L_3 phase. Since there is no L_1 phase present, it is no surprise that the plume has not been observed in two-phase samples.

E. Other features

We have performed a small number of experiments in which the temperature quench was reversed before the reor-

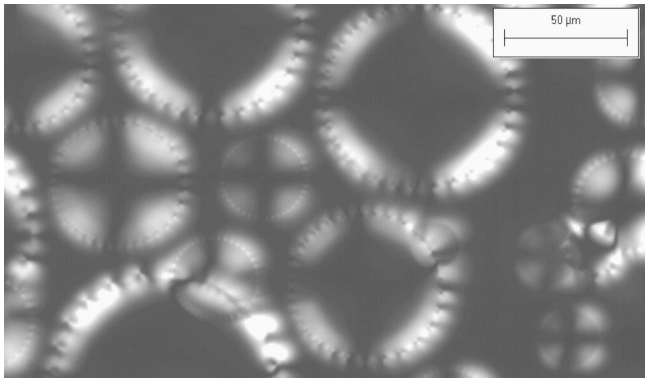

FIG. 19. After an increase in temperature, smectic bubbles are observed to form in the L_3 phase.

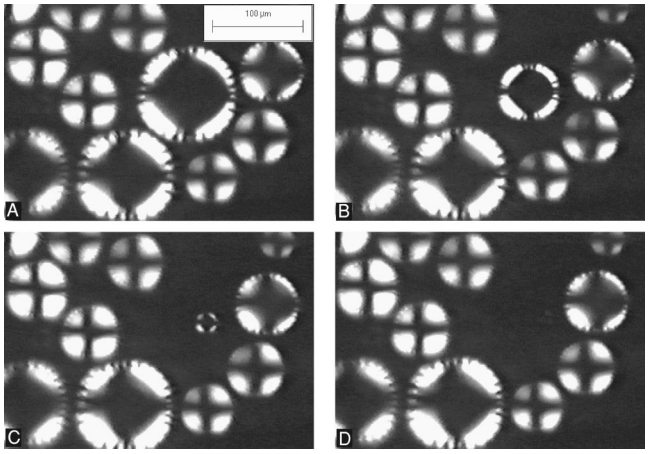

FIG. 20. One of the smectic bubbles ''bursts,'' and collapses rapidly to a point (over a period of about 1 s).

ganization of the phases was complete. During an *increase* in temperature, we have observed *smectic bubbles* in the L_3 phase. These are L_α films which contain focal conic defects (Fig. 19). Each bubble once contained a lamellar onion droplet suspended in the L_3 phase. On raising the temperature, the central region melts, and we observe changes in the birefringence of the bubble.

Eventually the bubble rapidly shrinks down into a small lamellar droplet (Fig. 20). In some cases we observe the bubble to rapidly collapse, and then completely vanish after it bursts. The kinetic behavior of such processes remains to be fully investigated.

V. CONCLUSION

Temperature quench experiments in surfactant systems have led to a variety of interesting observations. In the initial stages after the temperature quench, disruption of the L_3 phase occurs, and L_1 droplets are found to move from the L_α phase through the L_3 phase to the L_1 phase. This is attributed to a sudden reduction in the bilayer concentration which causes the L_3 and L_α phases to expel solvent, forming a ''sponge emulsion,'' and a suspension of L_1 droplets, respectively. This is only observed in the first few hours after the quench. After this rapid equilibration of the bilayer concentration, we observe the formation of lamellar droplets in the sponge phase close to the L_1/L_3 interface. This observation can be explained in terms of the evolution through a free energy landscape. As the system proceeds to equilibrium it goes through a series of metastable states. Under such conditions the bilayer concentration at the L_1/L_3 interface can be larger than at the L_α/L_3 interface. In this case the sponge phase is more likely to nucleate lamellar phase droplets close to the micellar-sponge interface. However until we can directly probe the density of the sponge phase as a function of sample height during this process this explanation remains speculative, and the inverted density profile of Fig. 18 remains a conjecture.

At a later stage we observe a plume to form at the L_1/L_3 interface which connects to the L_α phase. This may be due to the nucleation of lamellar phase droplets in the micellar phase L_1, which get ''stuck'' when they reach the sponge phase interface. If the surface tension of the L_α/L_3 interface is large, then the lamellar phase will build up until there is enough to break through. The break through is driven by gravity as in a lava lamp.

In two-phase samples which were prepared at a larger bilayer concentration, we have observed different features. The absence of the third phase (L_1) means that we do not observe nucleation at the bottom of the cell or the formation of the plume. This gives weight to the free-energy landscape explanation of the nucleation kinetics.

ACKNOWLEDGMENTS

We are grateful to P. Garrett, D. Roux, J. Leng, G. Tiddy, J. Walsh, and P. Warren for useful discussions. L.S. thanks the Institute of Food Research for financial support. M.B. thanks Unilever PLC and EPSRC (UK) for financial support. This work was funded in part under EPSRC Grant No. GR/K59606.

[1] S. Egelhaaf, Curr. Opin. Colloid Interface Sci. **3**, 608 (1998).
[2] S. Egelhaaf and P. Schurtenberger, Phys. Rev. Lett. **82**, 2804 (1999).
[3] J. Morris, U. Olsson, and H. Wennerström, Langmuir **13**, 606 (1997).
[4] S. Egelhaaf *et al.*, Phys. Rev. E **60**, 5681 (1999).
[5] D. Siegel and R. Epand, Biophys. J. **73**, 3089 (1997).
[6] J. Vollmer and D. Vollmer, Faraday Discuss. **112**, 51 (1999).
[7] D. Vollmer and J. Vollmer, Physica A **249**, 307 (1998).
[8] R. Virchow, Virchow's Archive **6**, 562 (1854).
[9] R. Laughlin, *The Aqueous Phase Behaviour of Surfactants* (Academic Press, New York, 1994).
[10] A. Sein, Ph.D. thesis, University of Groningen, 1995 (unpublished).
[11] I. Sakurai, T. Suzuki, and S. Sakurai, Biochim. Biophys. Acta **985**, 101 (1989).

[12] I. Sakurai and Y. Kawamura, Biochim. Biophys. Acta **777**, 347 (1984).
[13] K. Mishima and K. Yoshiyama, Biochim. Biophys. Acta **904**, 149 (1987).
[14] I. Sakurai, T. Suzuki, and S. Sakurai, Mol. Cryst. Liq. Cryst. **180**, 305 (1990).
[15] L. Sallen, P. Oswald, and P. Sotta, J. Phys. II **7**, 107 (1997).
[16] R. Evans and W. Poon, Phys. Rev. E **56**, 5748 (1997).
[17] W. Poon *et al.*, Phys. Rev. Lett. **83**, 1239 (1999).
[18] R. Evans, W. Poon, and M. Cates, Europhys. Lett. **38**, 595 (1997).
[19] R. Evans, W. Poon, and M. Cates, Nuovo Cimento **20**, 2155 (1998).
[20] F. Renth, W. Poon, and R. Evans (unpublished).
[21] R. Evans, W. Poon, and F. Renth, J. Phys.: Condens. Matter **12**, 269 (2000).
[22] L. Starrs, Ph.D. thesis, University of Edinburgh, 1999.
[23] W. Poon *et al.*, Faraday Discuss. **112**, 143 (1999).
[24] C. Blanc and M. Kleman, Eur. Phys. J. B **10**, 53 (1999).
[25] R. Strey *et al.*, *Structure and Dynamics of Strongly Interacting Colloids and Supramolecular Aggregates in Solution* (Kluwer, Dordrecht, 1992), pp. 351–363.
[26] M. Buchanan, J. Arrault, and M. Cates, Langmuir **14**, 7371 (1998).
[27] W. Z. Helfrich, Z. Naturforsch. A **33A,** 305 (1978).
[28] M. Buchanan, S. Egelhaaf, and M. Cates, Langmuir **16**, 3718 (2000).